Radio Frequency-assisted Curing of On-chip Printed CNT/silicone Heatsinks Produced by Material Extrusion 3D Printing

Thang Q. Tran [a,b], Anubhav Sarmah [a], Ethan M. Harkin [a], Smita Shivraj Dasari [a], Kailash Arole [c], Matthew J. Cupich [a], Aniela J. K. Wright [a], Hang Li Seet [b], Sharon Mui Ling Nai [b], Micah J. Green [a,c,*]

[a] Artie McFerrin Department of Chemical Engineering, Texas A&M University, College Station, TX, 77843, USA

[b] Singapore Institute of Manufacturing Technology (SIMTech), Agency for Science, Technology and Research (A*STAR), 5 Cleantech Loop, #01-01 Cleantech Two Block B, Singapore 636732, Republic of Singapore

[c] Department of Materials Science and Engineering, Texas A&M University, College Station, TX, 77843, USA

*Corresponding author: E-mail: micah.green@tamu.edu (Micah J. Green)

Abstract

With the rapid development of high-power integrated electronic devices, many polymer-based thermal management devices have been developed to address the problem of overheating and to improve the reliability and lifetime of electronic devices. Here we demonstrate the material extrusion 3D printing of carbon nanotube (CNT)/silicone heatsinks directly onto electronic devices. CNTs were used as a conductive nanofiller and a rheological modifier to improve thermal and electrical conductivities and the printability of the silicone inks, respectively. Additionally, CNTs are also a radio frequency (RF) susceptor, so the integration of CNTs into the silicone matrix allowed for rapid out-of-oven curing by applying RF heating. Specifically, at a CNT loading of 14 wt.%, the CNT/silicone heatsinks could be printed and RF cured with shape retention; the heatsinks' performance was comparable to that of commercial heatsinks. More importantly, the CNT/silicone heatsinks could be printed and cured directly onto a chip attached to a circuit board. This printing approach can eliminate the use of thermal interface materials and the step of heatsink assembly while reducing the number of thermal interfaces between the chip and the heatsink. The results suggest that material extrusion 3D printing combined with RF-assisted curing can be an effective approach to fabricate high-performance polymer-based heatsinks with reduced production time and energy requirements.

Keywords: Material extrusion, carbon nanotube, radio frequency heating, silicone, heatsink

1. Introduction

Electronic devices have become more miniaturized and highly-integrated while having better capability to serve several functions with high performance [1, 2]. However, as these devices are miniaturized, the required power density of the electronic devices also increases, leading to overheating, which can lower the device performance, reliability, and lifetime [1, 3]. To address this issue, many thermal management materials (TMMs) have been developed to effectively dissipate the excess heat [1, 3-5]. They are used to fabricate heat exchangers (such as heatsinks, heat spreaders, and heat pipes) or thermal interface materials (TIMs) (such as thermal greases, thermal pastes, and thermal tapes) which are widely used in sectors such as aerospace, healthcare, and automotive [5-8].

TMMs can be categorized into metals, polymers, ceramics, and composite materials [5, 6, 9]. Despite the high thermal conductivity, metal- and ceramic-based TMMs have constrained processability, high density, and high cost [2]. The polymer-based TMMs, however, have great potential to replace their metal and ceramic counterparts in several thermal management applications; their advantages include light weight, excellent corrosion and chemical resistance, low cost, and ease of processing [2, 10]. It has been reported that some thermal management devices made of polymer-based and metal-based TMMs exhibited comparable thermal performance [11, 12]. Due to the low thermal conductivity of the neat polymers, thermally conductive nanofillers such as ceramic (e.g., boron nitride or aluminum oxide) and metal (e.g., aluminum, copper) particles are usually added to the polymer matrices to enhance their thermal performance [3-5]. Moreover, the addition of nanofillers can alter the rheological behaviors of the resulting nanocomposite solutions, which can offer better processability for several advanced manufacturing methods [13, 14].

Additive manufacturing (AM) or 3D printing is an advanced production method that allows new capabilities in material processing [13, 15, 16]. AM can fabricate highly complex parts with low cost, minimized material waste, and good customization [13, 15-17]. The advantages of AM methods can be employed to fabricate TMM devices with intricate geometries and high surface area for improved heat dissipation efficiency [1, 3, 4, 6]. In fact, many studies have reported the use of different AM methods to process polymer-based TMMs for thermal management applications [1, 3, 4, 11, 18-22]. In these studies, the polymer feedstocks of the AM printers are usually modified by adding different thermal conductive nanofillers such as carbon fibers [19, 20], copper nanoparticles [18, 23], and graphene nanoplatelets [3, 24]. Among these AM processes, direct ink writing (DIW) is one of the most widely used material extrusion AM techniques to fabricate thermoset-based TMM devices because DIW can be used to process a wide range of commercial thermoset matrices and nanofillers [13, 19, 20]. Moreover, this method can process highly viscous TMM inks at low printing temperature, offering the ability to print the TM devices on a wide range of substrate materials [13, 19, 20].

One major issue for DIW 3D printing of thermoset-based TMMs is the time-consuming curing process of the printed products [14, 25]. At room temperature, thermoset-based TMMs require several days to be fully cured [26, 27]. Although high curing temperature can shorten the curing time, the printed thermoset-based structures usually need to be cured at low temperatures for many hours to avoid structural collapse [14, 26]. Moreover, most research on DIW of thermoset-based TMMs reported the use of conventional heating ovens with low heating rate and long heating time [20, 26]. Moreover, the oven heating process usually requires high energy consumption (several hundreds Watts) and does not offer targeted heating which is crucial for some manufacturing processes and applications [14, 25].

Recently, our group has successfully applied radio frequency (RF) heating to improve the DIW process of carbon nanotubes (CNTs)/epoxy composites [13, 20]. Since CNTs are an excellent RF susceptor, the printed CNT/epoxy composites can be rapidly heated and cured by RF heating during the printing process, allowing reduced processing time and energy requirements [13, 20]. Compared to conventional heating methods, RF heating offers several benefits such as volumetric and targeted heating, faster heating rate, lower infrastructure requirements, and better energy efficiency [14]. More importantly, RF heating can offer out-of-oven processing of polymers. We have successfully applied this advanced heating technology to process thermosetting prepregs [28], fabricate carbon fiber composites [29, 30], cure pre-ceramic polymer composites [31], improve the inter-layer strength of 3D printed thermoplastics [32], weld thermoplastic surfaces together [33, 34], heat conductive fabrics [35], and reduce graphene oxide [36]. Therefore, RF heating technology has great potential to reduce the curing time of thermoset-based TMMs processed by DIW 3D printing.

3D printing of TMM heatsinks are usually conducted on a printbed, and the printed heatsinks are subsequently attached to electronic components by using TIMs such as thermal tape or thermal paste [5]. 3D printing heatsinks directly onto a chip would be highly advantageous: This approach would eliminate the use of TIMs, resulting in reduced material cost while improving the thermal performance of the heatsinks by reducing the number of thermal interfaces [5]. Moreover, because the heatsink would be formed directly on the electronic devices, the heatsink-device assembly process can also be eliminated, leading to improved process automation. Very few studies have reported the successful 3D printing of metal-based heatsinks on a bare chip [37], and 3D printing of polymer-based heatsinks on a chip attached to a circuit board has yet to be investigated.

In this paper, we aim to apply RF heating to speed up the curing process of CNT/silicone heatsinks printed by DIW 3D printing. Here, CNTs are used as a thermally conductive nanofiller and a rheological modifier to improve thermal conductivity and printability of the CNT/silicone composite ink. The heatsinks are printed both on a printbed and directly on a chip attached to a circuit board. As CNTs are RF susceptors, the integration of CNTs into the silicone matrix allows fast out-of-oven curing of the printed CNT/silicone heatsinks by applying RF heating. The performance of the printed heatsink is evaluated by using single-board computers and compared with a commercial Al heatsink. The results suggest that the DIW combined with RF-assisted curing process can an effective approach to fabricate high-performance polymer-based heatsinks with reduced production time and energy requirements.

2. Materials and Methods

2.1 Materials and formulation

The Sylgard^{TM}184 silicone elastomer was provided by VWR International (USA). It is a two-component system with a mixing ratio of 10 (base):1 (curing agent) by weight. The multi-walled carbon nanotubes (CNTs) were obtained from Cheap Tubes Inc. (USA). The CNT/silicone ink formulations were prepared by mixing silicone base, curing agent, and different amounts of CNTs at 2000 rpm in 2 mins using a planetary mixer (Thinky coporation, AR-100).

2.2 3D printing

Once formulated, the ink was manually loaded into a 15cc dual-gasket stainless steel cartridge of a DIW print head (Hyrel 3D, EMO-XT) by using a spatula. Filled cartridge was centrifuged at 5000 rpm for 30 min using a centrifuge (Thermo Fisher Scientific, Sorvall ST1 Plus) to remove air bubbles introduced during the ink loading process. Loaded cartridges were then attached to the print head mounted in a DIW printer (HyRel 3D, Engine SR) for printing experiments. The amount of extruded material is governed by the piston displacement [38]. Two nozzle sizes (0.41 and 0.84 mm) were used to dictate filament diameter for printing of small and large heatsinks. The CAD models of the printed specimens were sliced by Hyrel's Repetrel software to generate G-code files for printing. Important printing parameters are presented in **Table 1**. After the printing process is completed, the printed samples were transferred to the RF applicator for curing.

Table 1. Important printing parameters used for the printing process of CNT/silicone heatsinks

Parameters	**Small print**	**Large print**
Printing speed	1 mm/s	2 mm/s
Layer height	0.2 mm	0.4 mm
Extrusion width	0.41 mm	0.84 mm
Shell number	2	2
Infill Density	100%	100%
Infill overlap	5%	5%
Fill pattern	Rectilinear	Rectilinear
Infill angle	[45°/−45°]	[45°/−45°]

2.3 RF-assisted curing

An RF signal generator (Rigol inc, DSG815) and a 500 W amplifier (Prana R&D, GN500D) were employed to supply RF waves to a stationary, co-planar RF applicator for the curing process. The printed CNT/silicone samples were placed approximately 1 mm below the applicator and were heated to the curing temperatures by the electric field generated by the applicator. During the RF heating process, the RF power was varied between 0 to 30 W to control the heating temperature. Maximum temperature was recorded by using a thermal imaging infrared camera (FLIR Systems, Inc., A655sc).

2.4 Characterization

The rheological behavior of the CNT/silicone inks was characterized at ambient lab temperature (~25 °C) by using a stress-controlled rheometer (Anton Paar, MCR 301) fitted with a disposable plate–plate system (PP25, 25 mm diameter, 0.1 mm gap). The viscosity of the composite inks was measured as a function of shear rate (γ) (from 0.01 to 100 1/s), whereas their storage modulus (G′) and loss modulus (G″) were measured as a function of the shear stress (from 0.0001 to 10000 Pa) in oscillatory mode at a frequency of 1 Hz.

The cross-sectional morphologies of the printed CNT/silicone samples were investigated with a field emission scanning electron microscope (FE-SEM, Model Quanta 600 FEG, FEI Company). Samples for SEM observation were prepared by cutting the printed CNT/silicone samples with a sharp razor blade.

The through-plane AC conductivities of printed samples were measured by using a dielectric spectrometer (Novocontrol Technologies GmbH) at room temperature within the frequency range of 1 MHz to 10 MHz.

Thermal conductivity of the printed CNT/silicone samples was characterized by using a Thermal Conductivity Analyzer (Hot disk, TPS 2500S) which is based on transient plane source thermal characterization technique [40]. In this method, a 5465 Kapton-insulated sensor was used as a heat source and temperature sensor for all measurements. The sample being tested was cylindrical in shape, with diameter 12.7 mm and thickness 3.2 mm. To perform the measurement, the Kapton-insulated sensor was sandwiched between two pieces of CNT/silicone sample. An electrical current was then applied to the sensor to increase its temperature. The temperature increase as a function of time was recorded and then was used to determine the thermal conductivity of the tested samples.

To qualitatively evaluate the heat dissipation ability of the CNT/silicone samples, the thermal camera was employed to capture the surface temperature response of the samples heated by a hotplate at 80 °C.

Differential scanning calorimetry (DSC, TA Instrument DSC2000) was conducted in Nitrogen from 25 °C to 350 °C at a heating rate of 10 °C/min.

2.5 Heatsink performance

Heatsink performance was characterized by measuring temperature of a CPU chip attached to a single-board computer (Raspberry Pi 4 model B, 2 GB) purchased from McMaster-carr. A thermal tape of 250 µm thickness and thermal conductivity of 1.1 W/m.K (McMaster-carr) was used to attach the on-printbed printed CNT/silicone heatsinks and commercial Al heatsink to the top of the CPU chip. Under natural convection, the CPU chip temperature was measured as a function of time by using a Python script.

3. Results and discussion

3.1 Printability of CNT/silicone ink

In this study, CNTs are used as a viscosifier to modify the rheology and improve the printability of the silicone-based ink formulation. **Figs. 1a and b** show rheological properties of CNT/silicone inks at varying CNT loading. The viscosity of the neat silicone ink (0 wt.% CNT) is nearly independent of shear rate, indicating a Newtonian behavior (**Fig. 1a**). With the addition of CNTs, the viscosity of the inks increased across all tested shear rates. Specifically, the ink viscosity at the shear rate of 2×10^{-2} 1/s increased significantly from 0.5 Pa.s for 0 wt.% CNT to 10^2 Pa.s for 8 wt.% CNT and 1.1×10^5 Pa.s for 12 wt.% CNT. However, when CNT loading increased from 14 to 16 wt.%, the effect of CNT loading on the viscosity of the inks was less significant with an increase in viscosity to only 2.2×10^5 Pa.s for 16 wt.% CNT at the shear rate of 2×10^{-2} 1/s. The CNT loading of more than 16 wt.% does not form a homogeneous CNT/silicone mixture and, therefore, it was not employed for DIW printing in this study. Notably, the inks with CNT loading from 8 wt.% to 16 wt.% exhibited shear thinning behavior with the viscosity reducing at increasing shear rate. This non-Newtonian behavior is critical for DIW 3D printing because it allows the viscous inks to flow through the printer nozzles under high shear stress without requiring excessive applied pressure [14, 26].

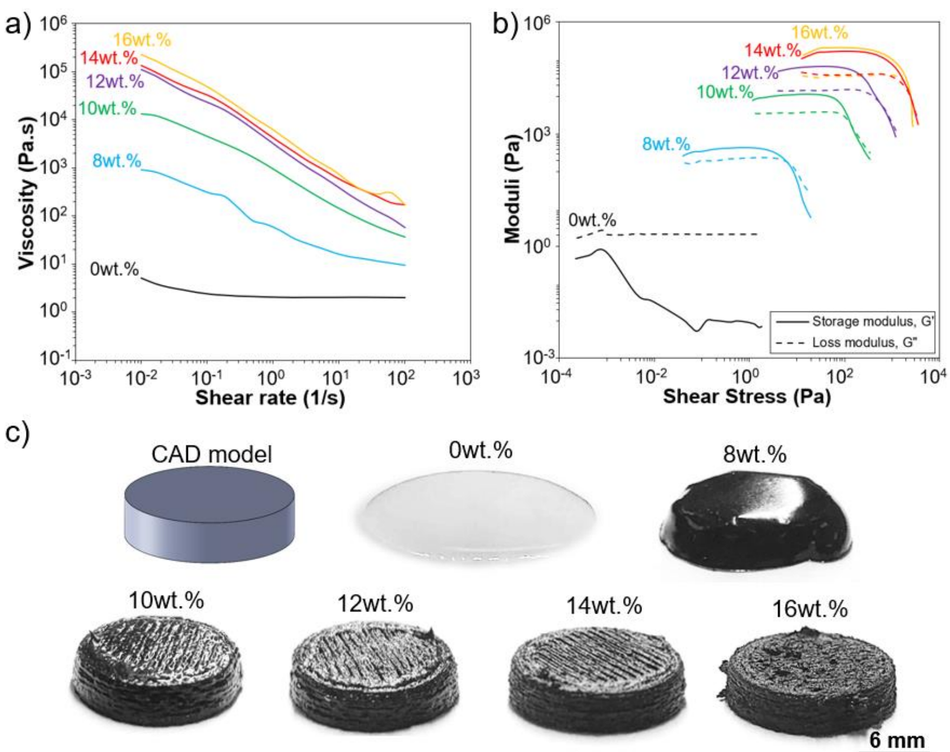

Fig. 1. Log-log plots of (a) apparent viscosity as a function of shear rate and (b) shear storage and loss moduli as a function of shear stress for CNT/silicone inks at varying CNT loadings. (c) CNT/silicone coins printed at different CNT loadings.

Once the ink is extruded from the printing nozzle, the shear stress is removed and the ink must return to solid-like behavior to maintain its shape retention. This property can be characterized by measuring the storage modulus (G′) and loss modulus (G″) of the inks [26]. As shown in **Fig. 1b**, the shear storage modulus of the neat silicone ink was lower than its loss modulus, indicating that neat silicone ink exhibited liquid-like behavior throughout the tested range of shear stress. For CNT loadings from 8 wt.% to 16 wt.%, the inks exhibited a shear yield stress at the crossover point between the two modulus curves. Specifically, the shear yield stress of the 8 wt.% CNT/silicone inks was only 7.5 Pa. When the CNT loading increased to 14 wt.%, the shear yield stress of the inks increased significantly to 3000 Pa. Moreover, the storage and loss moduli below the yield stress also increased from 4×10^2 Pa and 2×10^2 Pa for 8 wt.% CNT to 2×10^5 Pa and 5×10^4 Pa for 14 wt.% CNT, respectively. Similar to the viscosity, the increase of CNT loading from 14 wt.% to 16 wt.% had insignificant effects on the yield stress and moduli of the inks. For good shape retention after deposition, the composite inks must have sufficient yield stress for rapid recovery of high viscosity and elastic behavior [14, 26].

Fig. 1c show coins printed by DIW using CNT/silicone inks at different CNT loading. Due to the low viscosity, the neat silicone ink could readily flow through the printer nozzles under low driving pressure. However, the printed ink could not support itself and immediately spread on the printbed upon exiting the nozzle as it possessed liquid-like behavior. At 8 wt.% CNT, the printed structure could maintain its shape with less spreading of the lower layers. However, filaments still can flow and coalesce during deposition, resulting in printed parts with a smooth surface and geometric distortion. These results might be due to the low yield stress of the 8 wt.% CNT/silicone ink, which was still insufficient for good shape retention [14, 26]. As CNT loading increases from 10 to 16 wt.%, the inks have much higher shear yield stress (>1600 Pa) and, therefore, the printed coins possess good shape retention with consistent dimension [26]. Additionally, the surface features of the printed coins became sharper, and all layers and filaments are more defined and visible on the exterior surface. However, excessive applied pressure was required to process the 16 wt.% CNT formulation due to its significantly high shear yield stress [40]. Moreover, the extrudates of the ink formulation could not be deformed easily during the printing process to achieve good coalescence between adjacent filaments. Consequently, several excessive extrudates were accumulated at the surface of the printed part, resulting in their low surface quality.

3.2 Cross-sections of the printed CNT/silicone samples

To investigate the structure of printed CNT/silicone composites, the cross-sections of the printed composites were characterized with SEM. **Fig. 2** shows the cross-sections of printed CNT/silicone samples with a CNT loading from 10wt.% to 16 wt.%. CNTs are uniformly embedded in the silicone matrix with no CNT agglomerates observed in any samples. As the CNT loading increased, the amount of CNTs observed at the cross section also increased, whereas excellent dispersion property of CNTs in the silicone matrix still could be maintained. The result suggests that the dispersion process used in this work can successfully generate CNT/silicone inks with good dispersion quality. Notably, there were no voids/gaps observed in the cross-sections of the inks with CNT loading from 10 to 14 wt.%, as shown in **Figs. 2a, d, and g**. The result suggests that the degassing process was efficient, and no voids/gaps were introduced into the printed structure during the printing process of these inks. Additionally, the ink viscosities are still sufficiently low to allow the extruded materials to flow and completely fill the void space between the adjacent filaments. However, several internal voids can be observed at the cross-section of the structure printed with 16 wt.% CNT formulation. This can be explained by the fact that the significantly high viscosity of the inks reduces the efficiency of the degassing process and coalescence between the adjacent filaments [40]. This result is consistent with formation of voids in silicon nitride structures printed by DIW using high viscosity inks [40].

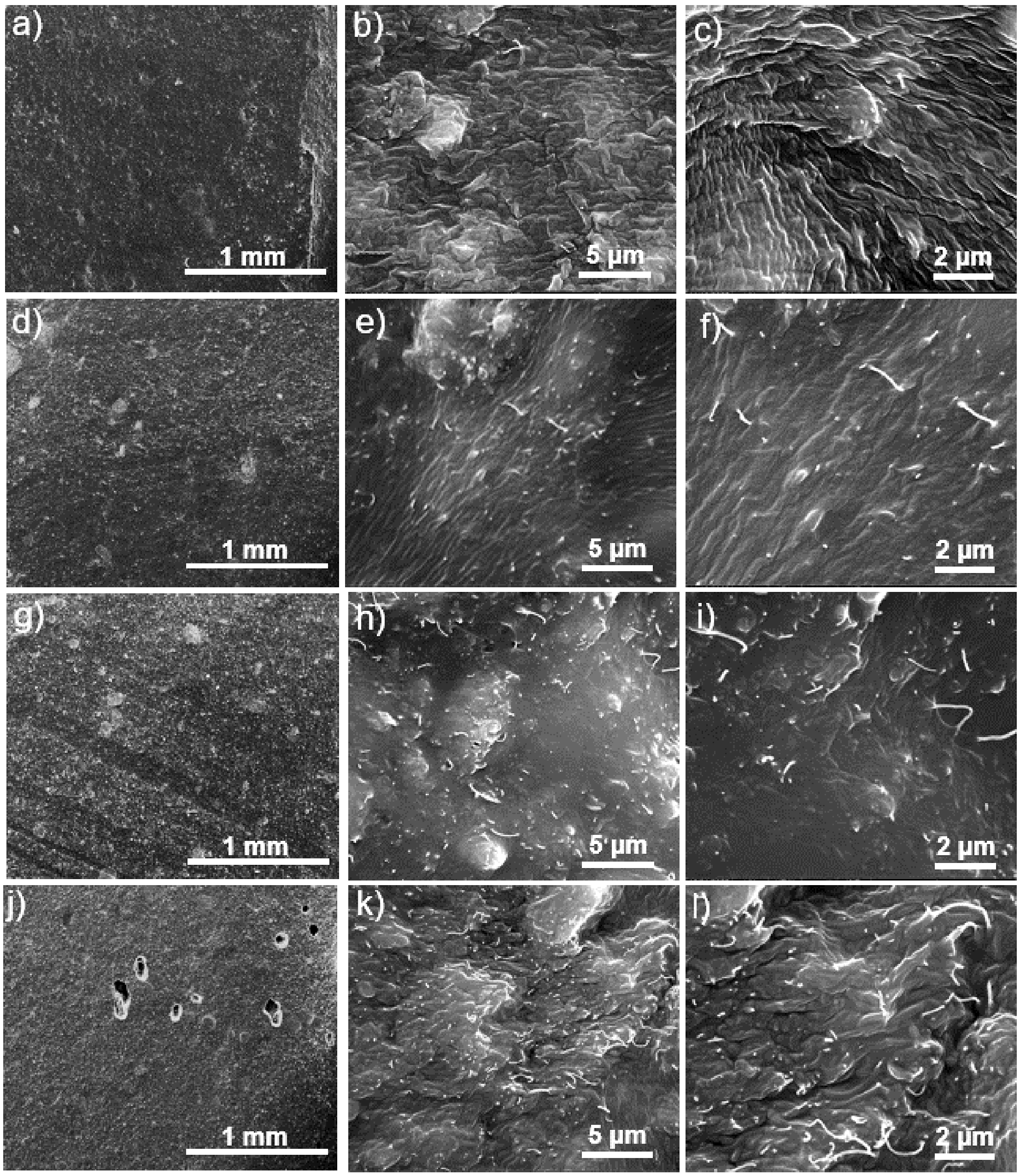

Fig. 2. Cross-sections of the printed CNT/silicone samples at 10wt.% CNT (a, b, c), 12wt.% CNT (d, e, f), 14wt.% CNT (g, h, k), and 16wt.% CNT (j, k, l).

3.3 Electrical and thermal properties of printed CNT/silicone samples

To explore the reinforcement effects of CNT filler on the performance of the printed CNT/silicone structures, thermal and electrical properties of the printed composite structures were investigated. Due to the low viscosity, neat silicone (0 wt.% CNT) were cast into a printed molds to fabricate samples for the characterization. **Fig. 3a** shows the AC electrical properties of the CNT/silicone samples from 1 to 10 MHz. Silicone possesses an electrical conductivity of below 5.5×10^{-15} S/cm in the tested frequency range and the frequency has insignificant effects on the electrical performance. With the addition of CNT fillers, the electrical conductivity of the samples significantly improved with higher CNT loading offering better electrical conductivity. The results are expected because electrical conductivity of CNTs is significantly higher than that of the silicone and CNTs have been widely used as electrical conductive reinforcement nanofiller to improve the electrical conductivity of the insulating matrix [5]. Additionally, the electrical conductivity of the CNT/silicone samples exhibited frequency dependent behavior. Specifically, when the applied frequency increased from 1 to 10 MHz, the electrical conductivity of samples with 10 and 12 wt.% CNT increased by 160% and 133%, reaching 0.13×10^{-3} S/cm and 0.28×10^{-3} S/cm, respectively. The effects of the frequency on the electrical performance of the composite samples were more significant at higher CNT loading with an increase of approximately 5 times and 12 times for 14 wt.% and 16 wt.% CNT samples in the tested frequency range, respectively. The increase of AC electrical conductivity with increasing frequency is well-known response for polymer and polymer composite and was explained by an increase of the electron mobility with applied field frequency [41].

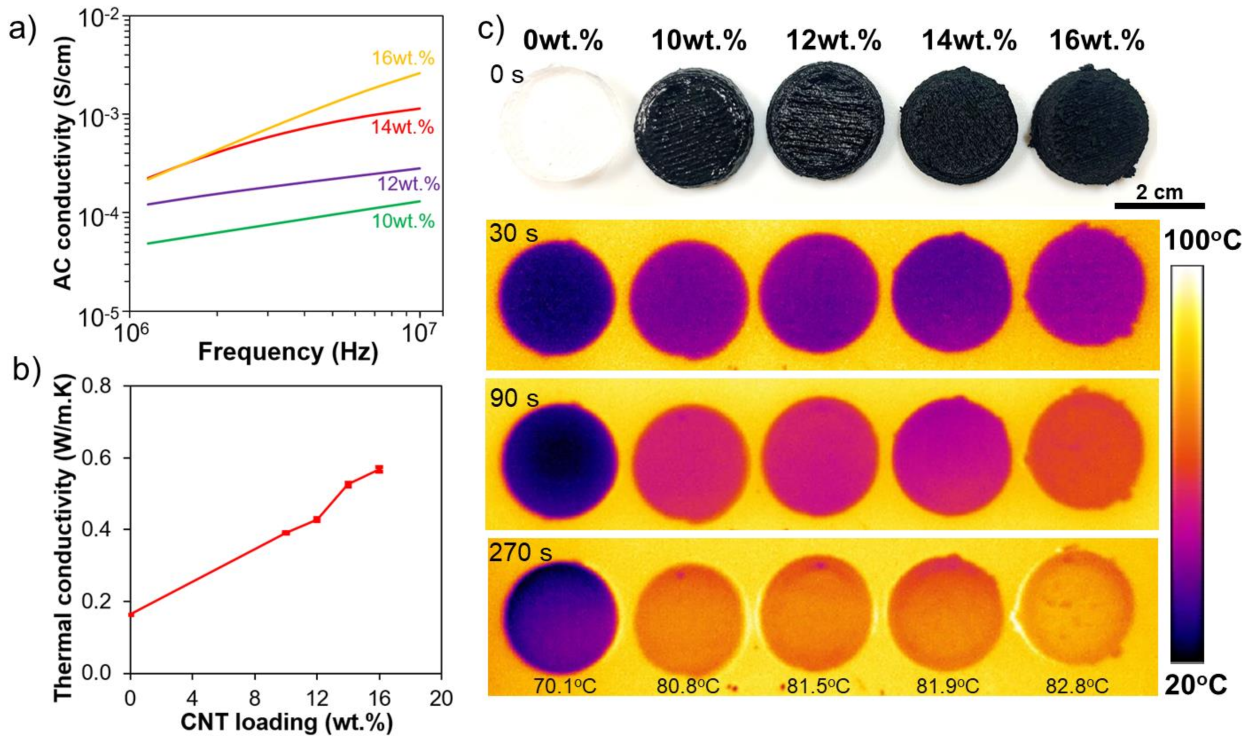

Fig. 3. AC conductivity (a), thermal conductivity (b), and (c) infrared thermal images of the printed CNT/silicone samples with increasing heating time when the samples were employed as a heat transfer medium. Maximum temperature of each sample at 270 s is presented in the corresponding IR thermal image. Neat silicone samples were casted in a mold while the other samples were printed.

Fig. 3b shows the effects of CNT loading on the thermal conductivity of the silicone-based samples at different CNT loading. Neat silicone possessed a low thermal conductivity of approximately 0.164 W/m.K. The addition of 10 wt.% CNT could increase the thermal conductivity of the sample to 0.392 W/m.K, corresponding to an increase of 139%. Further increase of CNT loading results in the gradual increase of the thermal conductivity to 0.428 W/m.K for 12 wt.% CNT, 0.526 W/m.K for 14 wt.% CNT, and 0.568 W/m.K for 16 wt.% CNT.

The difference in the surface thermal responses of the CNT/silicone samples with heating time is presented in **Fig. 3c**. The surface temperature of the composites samples with higher CNT loading exhibited faster response due to better thermal conductivity. Specifically, the surface temperature of the 16 wt.% CNT/silicone samples can reach 83 ºC after 270 s, whereas neat silicone samples only can achieve a temperature of 71 ºC. The results suggest CNTs can significantly improve the heat transfer capacity and the heat dissipation performance of the silicone matrix. Notably, despite pores and voids in the sample structures (**Fig. 3j**), the 16 wt.% CNT/silicone samples still have the highest electrical and thermal conductivity. The finding suggests that the effects of voids and pores on the electrical and thermal performance of the samples are less significant compared to the reinforcement effects of the CNT fillers. However, due to required excessive applied pressure for printing and the poor surface quality of the printed sample, 16 wt.% CNT/silicone inks were not used for the 3D printing of heatsink in this study. The 14 wt.% CNT/silicone inks, however, have better printability and surface quality with good thermal and electrical conductivity. Therefore, 14 wt.% CNT composites were used to print heatsinks for RF curing study in the next sections.

3.4 RF-assisted curing of printed CNT/silicone heatsinks

3.4.1 Heating response and RF curing of 14 wt.% CNT/silicone samples

Since the 14 wt.% CNT formulations have good electrical conductivity, we hypothesized that these samples can be heated rapidly in response to RF fields. **Fig. 4** presents the heating response of 14 wt.% CNT/silicone samples exposed to RF field at frequency of 160 MHz. The samples can be heated rapidly to targeted temperatures of 65, 100, and 150 ºC by using a heating power of 0.35, 0.75, and 1.25 W, respectively. Higher power can achieve not only higher targeted temperature but also faster heating rate [42]. Specifically, the power of 1.5 W can heat the samples at the highest heating rate with a value of up to 17 ºC/s. The volumetric heating (inside-to-outside) and faster heating rate of the RF heating, therefore, can accelerate the curing procedure of the printed CNT/silicone samples significantly compared to the oven heating [14, 25, 28, 29].

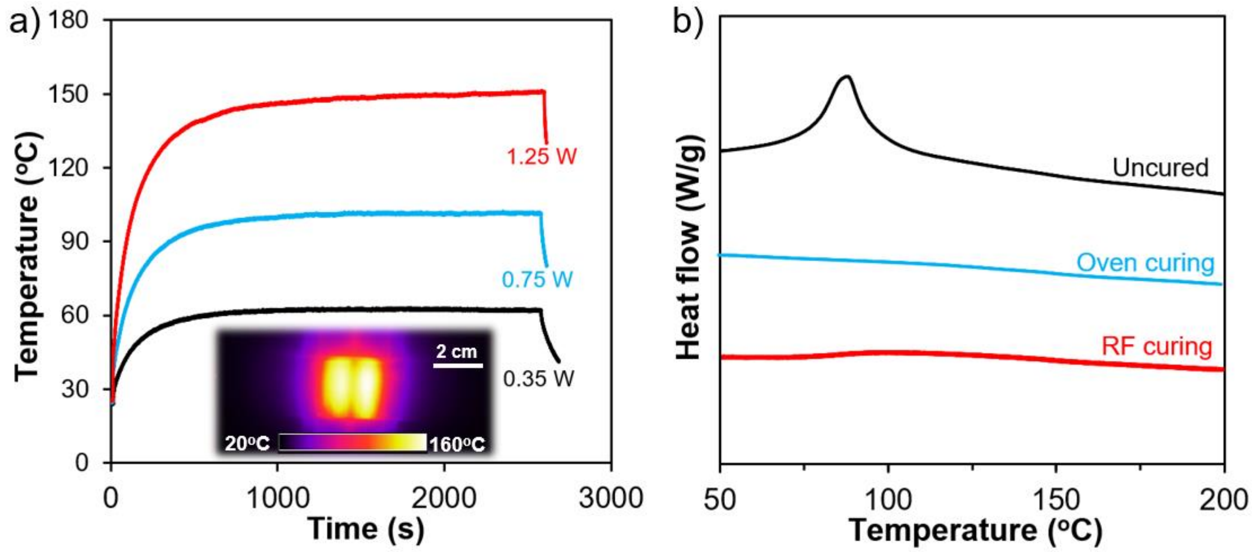

Fig. 4. a) Heating response of 14 wt.% CNT/silicone samples at different heating power. b) DSC thermographs of uncured 14 wt.% CNT/silicone samples and samples cured at 150 ºC in 10 mins by using heating oven and RF heating**.**

To confirm curing, we compared the DSC curves of uncured samples and sample cured by oven and RF heating at 150 ºC in 10 mins (**Fig. 4b**). The targeted temperature can be achieved by RF heating after 10-15 mins by using a single power value. Notably, this heating time can be shortened further to a few seconds by using high heating power (>1.5 W) at the beginning and then lowering the power to the desired value (1.5 W) to achieve the targeted temperature. The commercial heating oven used for the curing process, however, could require a longer time (~ 30−45 mins) and much higher power (1500 W) to achieve the same targeted temperature. The DSC curve of the uncured silicone composite samples presents one exothermic peak in the range between 80 and 100 ºC. This peak is associated with the curing reactions of the silicone polymer [27]. However, no exothermic peaks were observed in their DSC curves of the samples cured by oven and RF heating, indicating that the composite samples have been cured completely. The results suggest that RF heating is as effective as oven heating in curing the CNT/silicone composite. Therefore, this method will be used to cure the silicone heatsink printed by DIW in the next section.

3.4.2 On-printbed 3D printing and RF curing of 14 wt.% CNT/silicone heatsink

To demonstrate the potential of the 14 wt.% CNT/silicone inks for TM applications, different heatsinks were printed by DIW method and RF heating was applied to cure the printed structure at approximately 150 ^{o}C in 10 mins (**Figs. 5 a and b**). As shown in **Figs. 5c-f**, heatsinks with different designs and sizes could be fabricated, including conventional plate fin heatsink and nonconventional porous heatsink, and plate fin heatsink with TAMU logo shape and porous heatsink with A*STAR logo shape. The small size heatsinks can be used to dissipate heat from small electronic components such as CPU chips and power transistors. Overheating issues for large components such as light emitting diode (LED) lights and computer random-access memory (RAM) can be addressed by using the large printed heatsinks.

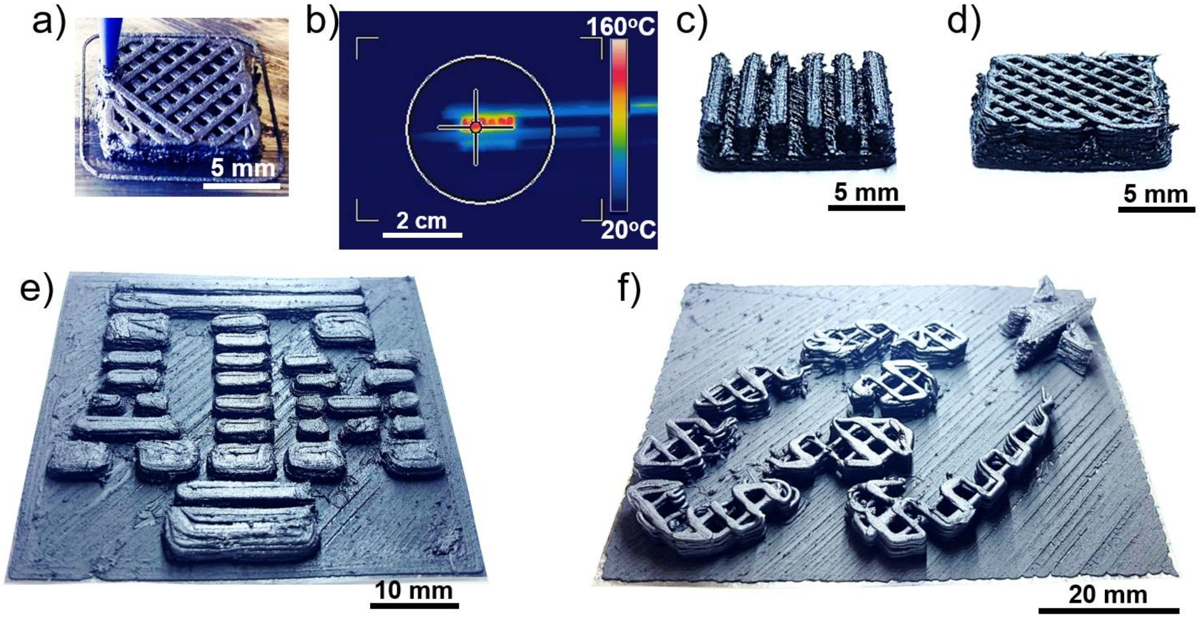

Fig. 5. a) 3D printing and b) RF curing of 14 wt.% CNT/silicone heatsink. 14 wt.% CNT/silicone heatsink with different designs and shapes: c) Conventional plate fin heatsink, d) nonconventional porous heatsink, e) plate fin heatsink with TAMU logo shape, and f) porous heatsink with A*STAR logo shape.

3.4.3 On-chip 3D printing and RF curing of 14 wt.% CNT/silicone heatsink

DIW 3D printing can be employed to print the heatsink directly on the surface of electronic devices. **Fig. 6** presents the printing process of a 14 wt.% CNT/silicone heatsink directly on a CPU chip of a Raspberry pi board. Although the CPU chip has a maximum size of up to 15×15 mm^2, its top surface is smaller (11×11 mm^2). Therefore, a smaller heatsink with a size of 10×10×3 mm^3 was printed on the chip to ensure that it can fit on the chip surface. The fin size and fin spacing of the on-chip printed heatsink were kept similar to the Al heatsink but the fin number and the fin length reduced to 5 and 10 mm, respectively, due to its smaller base size. The extruded filaments can attach properly to the chip surface with consistent flow and uniform filament shape. The viscosity of the 14 wt.% CNT/silicone ink was still sufficiently low so that the uncured filaments could be deformed under the pressure generated by the nozzle tip and the chip surface. Therefore, good contact can be achieved between the first printed layer and the chip surface for efficient heat transfer between the chip and the heatsink with no TIM.

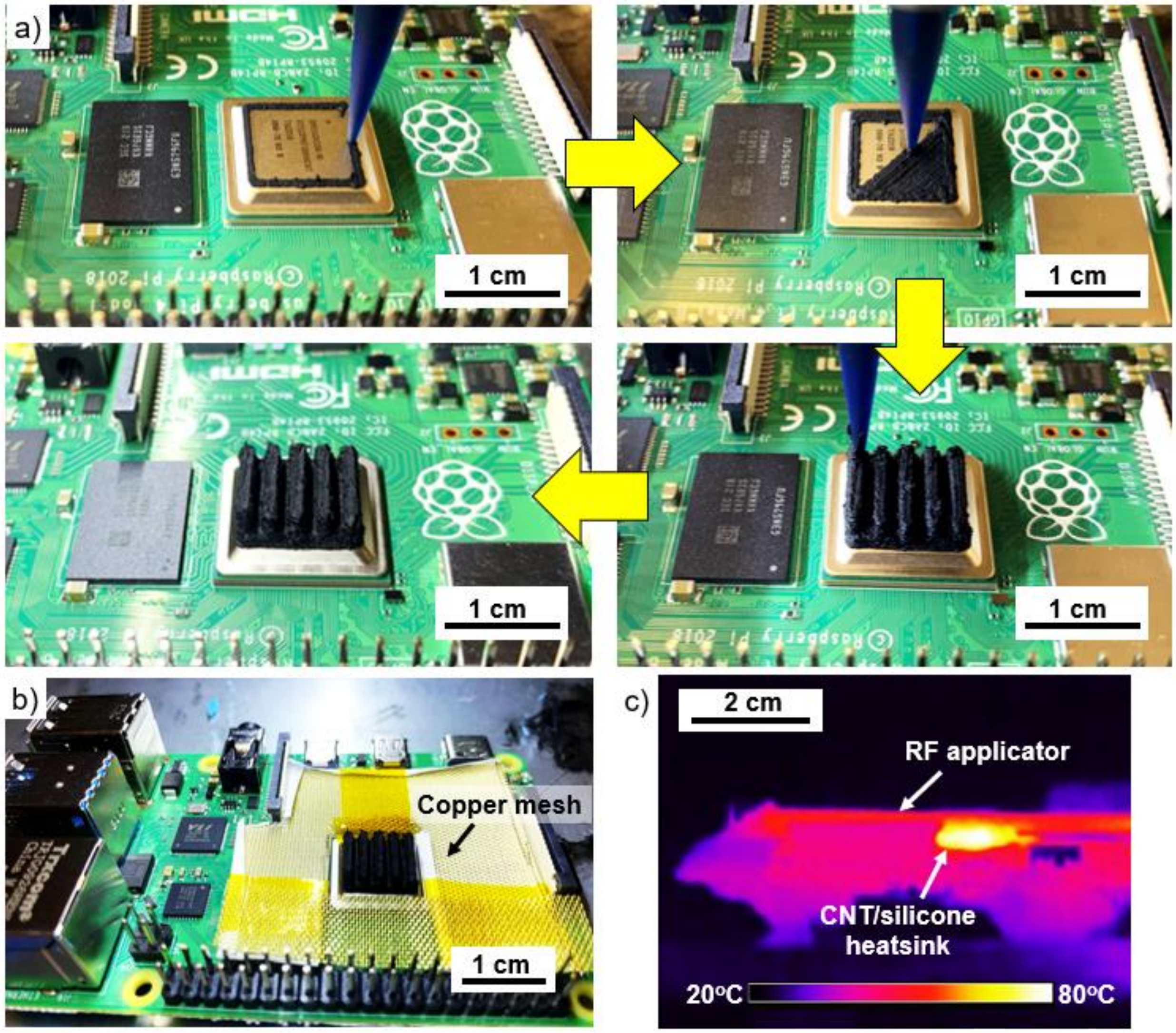

Fig. 6. a) Direct printing of 14 wt.% CNT/silicone heatsink on the CPU chip of a Raspberry pi board, b) Installation of copper mesh on the Raspberry pi board, and c) RF curing of the on-chip printed heatsink.

The printing process was quite consistent and reliable with no excessive extrudates observed on the circuit board. While the conventional fabricated heatsink are fabricated and installed on the chip separately, the on-chip printing of heatsink combined the two processes together and no further installation steps are required. Therefore, this printing approach can offer advantages in term of process automation. Comparing to the conventional installation method, this advanced printing approach can reduce the number of thermal interfaces formed between the heatsink and the chip surface, enhancing their heat transfer efficiency. The result suggests that 3D printing of CNT/silicone heatsink directly on a chip is feasible.

Most electronic components are designed to work in a temperature range of 40 °C to 50 °C [43]. If oven heating is employed for the curing process, the whole circuit board needs to be heated to the curing temperature and, therefore, only temperature below 50 °C can be used. This low curing temperature could increase the curing time to several hours, and a large amount of energy is required for the long oven curing process [44]. In RF curing process, a fringe electric field was generated by the RF applicator and mainly occurred within the 20 cm wide region between the copper traces. By targeting the RF field on the printed heatsink, local heating can be achieved to only heat the printed heatsink to the curing temperature with a low power [14]. A mask made of copper mesh was used to protect the circuit board and expose the heatsink to the RF field, as presented in **Fig. 6b**. Since most CPU chips can withstand a temperature of up to 85 °C [45], a heating temperature of 75−80 °C was used to cure the on-chip printed heatsink. As can be seen in **Fig. 6c**, only printed heatsink were heated to ∼ 75−80 °C under RF field at a frequency of 160 MHz and a power of 10 W. Compared to the curing temperature offered by the oven curing process, this higher curing temperature of the RF heating can shorten the curing time to ∼ 45 minutes [44].

Figs. 7 a-d show an on-chip printed heatsink, a small on-printbed printed heatsink, a large on-printbed printed heatsink, and a commercial Al heatsink attached to the surface of the CPU chip of the Raspberry pi board. While the on-chip printed heatsink was attached directly to the chip during the printing process, a 250-μm-thick thermal tape was used to install the on-printbed printed heatsinks, and Al heatsink. Notably, both large on-printbed printed heatsink and Al heatsink have similar design (6 fins) and dimension (13×13×3 mm), whereas the on-chip printed heatsink has less fin number (5 fins) and smaller size (10×10×3 mm) due to the size constraint of the chip surface. To investigate effect of the reduced thermal interface achieved by the on-chip printing process, a small on-printbed printed heatsink with a similar size was also fabricated.

Figs. 7 e and f present the temperature of the chip recorded at 2 conditions: 5% and 97% CPU usage. The chip temperature in **Fig. 7f** was the averaged temperature in the last 100 s of the testing period when the chip temperature was stabilized. All heatsinks can reduce the temperature of the CPU chip in both working conditions. Specifically, the chip without heatsink has a temperature of ~44.9 °C at 5% CPU usage and its temperature increased to 66.9 °C at 97% CPU usage. The installation of the small on-printbed printed heatsink can reduce the chip temperature to 43.9 and 63.9 °C for 5% and 97% CPU usage, respectively. The average temperatures of the on-chip printed heatsink are slightly lower than those of the small on-printbed printed counterparts, showing the advantage of the reduced thermal interface offered by the on-chip printing process. The on-printbed printed heatsink could even reduce the chip temperature further to 40.9 °C for 5% CPU usage and 60.8 °C for 97% CPU usage. The better performance of the on-printbed printed heatsink is expected as it had larger size and more fin number [46, 47].

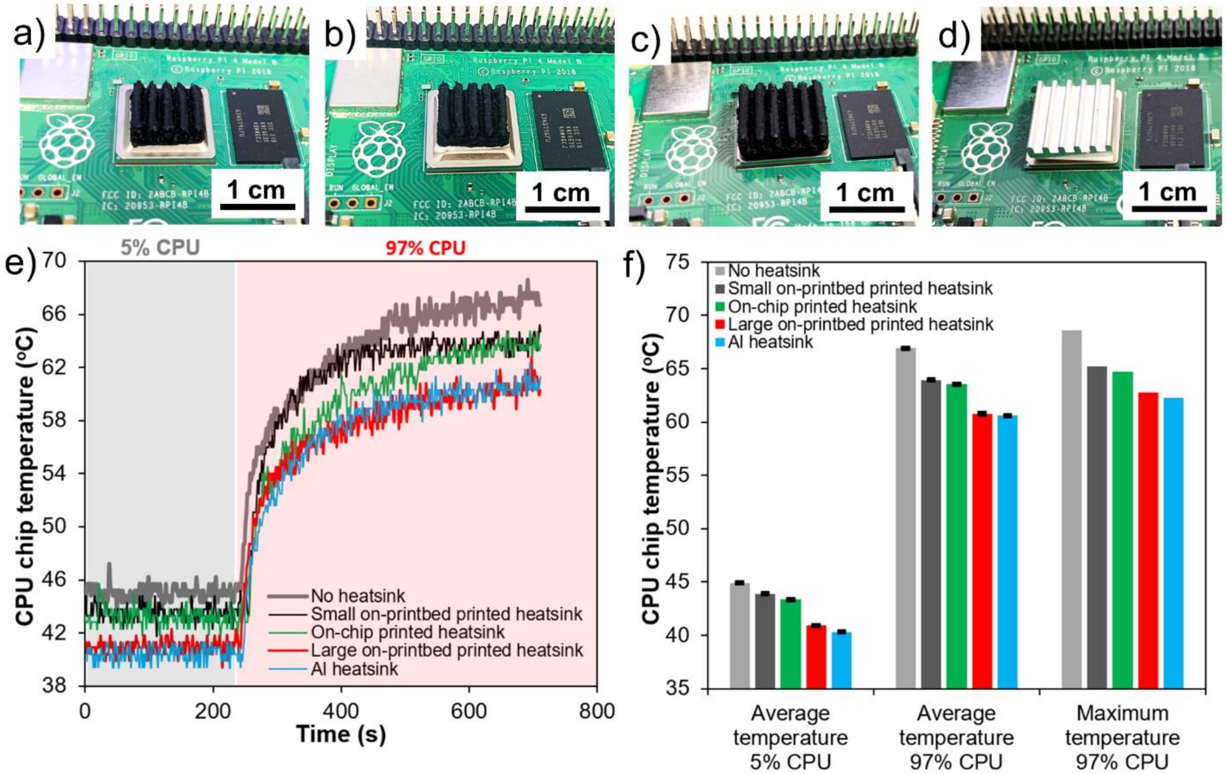

Fig. 7. Heatsinks installed on the CPU chip of a Raspberry pi board: a) On-chip printed CNT/silicone heatsink, b) small on-printbed printed CNT/silicone heatsink, c) large on-printbed printed CNT/silicone heatsink, and d) commercial Al heatsink. Temperature of the CPU chip at 5% and 97% CPU usage: e) temperature as a function of time and f) average temperature and maximum temperature in the last 100 s of the tested period.

Interestingly, there are no significant differences in the temperature of the chip installed with the on-printbed heatsink and the Al heatsink. Specifically, the temperature of the chip with Al heatsink was 40.3 and 60.6 °C for 5% and 97% CPU usage. Notably, the convection coefficient between the Al and on-printbed printed heatsinks should be very similar as they have the same shape, size, and gap between the fins [11, 12]. While the thermal conductivity of the CNT/silicone heatsink is much lower than that of the Al heatsink, their performance is comparable due to the limited role of conduction in heat removal under natural conduction [11, 12]. The result is in good agreement with the results reported by Smith *et al.* [11] and Guo *et al.* [12] when polymer heatsink printed by Fused Filament and a commercial Al heatsink with the same design and size exhibited similar performance under national convection.

4. Conclusion

In summary, we fabricated CNT/silicone heatsinks by using DIW 3D printing and RF-assisted curing processes. CNTs were employed as nanofiller to improve the electrical and thermal conductivities as well as the printability of the CNT/silicone composite inks and their printed structures, respectively. Among different CNT formulations used in the study, it was found that 14 wt. % CNT/silicone inks can be used to fabricate printed structure with good print quality and high thermal and electrical performance. Moreover, since CNTs are also a RF susceptor, the printed CNT/silicone heatsinks can be rapidly heated when exposure to RF fields, allowing them to be cured by the rapid out-of-oven RF heating process. Under natural convection, the printed CNT/silicone heatsinks exhibited similar performance to that of commercial heatsinks. More importantly, we have demonstrated that CNT/silicone heatsinks can be printed and cured directly on a chip attached to a circuit board. By applying this advanced approach, the installation step of the heatsinks with the use of TIMs can be eliminated while the thermal interfaces between the heatsink and the chip can be reduced. This work demonstrates that the DIW combined with RF-assisted curing process has the potential to produce high-performance polymer-based heatsinks for modern electronic applications.

CRediT authorship contribution statement

Thang Q. Tran: Conceptualization, Methodology, Investigation, Writing – original draft, review & editing. **Anubhav Sarmah**: Investigation. **Ethan Harkin**: Investigation. **Smita Dasari**:

Investigation. **Kailash Arole**: Investigation. **Matthew Cupich**: Investigation. **Aniela Wright**: Investigation. **Hang Li Seet**: Writing–review & editing. **Sharon Mui Ling Nai**: Writing- –review & editing. **Micah J. Green**: Conceptualization, Writing –review & editing.

Declaration of competing interest

The authors declare that they have no known competing financial interests or personal relationships that could have appeared to influence the work reported in this paper.

Acknowledgments

The authors acknowledge A*STAR Graduate Academy - A*STAR International Fellowship Program for their sponsorship. The authors thank the Materials Characterization Facility (RRID:SCR_022202) for the thermal conductivity and AC electrical conductivity measurement setups. Use of the Texas A&M University Soft Matter Facility (RRID:SCR_022482) for DSC is acknowledged. The authors thank the Materials and Testing Lab at TAMU for their Mechanical Testing setup and the Microscopy and Imaging Center at TAMU for SEM.

Supporting Information

STL files associated with the 3D prints in this manuscript are available in Supporting Information.

References

[1] S. Ligati Schleifer, O. Regev, Additive manufacturing of anisotropic graphene-based composites for thermal management applications, Addit. Manuf. 70 (2023) 103567.

[2] H. Zhang, T. Shi, A. Ma, Recent Advances in Design and Preparation of Polymer-Based Thermal Management Material, Polymers 13 (2021) 2797.

[3] Z. Peng, Q. Lv, J. Jing, H. Pei, Y. Chen, E. Ivanov, FDM-3D printing LLDPE/BN@GNPs composites with double network structures for high-efficiency thermal conductivity and electromagnetic interference shielding, Compos. Part B Eng. 251 (2023) 110491.

[4] J. Gao, M. Hao, Y. Wang, X. Kong, B. Yang, R. Wang, Y. Lu, L. Zhang, M. Gong, L. Zhang, D. Wang, X. Lin, 3D printing boron nitride nanosheets filled thermoplastic polyurethane composites with enhanced mechanical and thermal conductive properties, Addit. Manuf. 56 (2022) 102897.

[5] X. Guo, S. Cheng, W. Cai, Y. Zhang, X.-a. Zhang, A review of carbon-based thermal interface materials: Mechanism, thermal measurements and thermal properties, Materials & Design 209 (2021) 109936.

[6] S.A. Niknam, M. Mortazavi, D. Li, Additively manufactured heat exchangers: a review on opportunities and challenges, Int. J. Adv. Manuf. Technol. 112 (2021) 601-618.

[7] Z. Yuan, H. Ma, M.A. Hussien, Y. Feng, Development and Challenges of Thermal Interface Materials: A Review, Macromol. Mater. Eng. 306 (2021) 2100428.

[8] T.Q. Tran, A. Chinnappan, J.K. Lee, N.H. Loc, L.T. Tran, G. Wang, V.V. Kumar, W.A.D.M. Jayathilaka, D. Ji, M. Doddamani, S. Ramakrishna, 3D Printing of Highly Pure Copper, Metals, 2019, p. 756.

[9] P. Liu, Z. Fan, A. Mikhalchan, T.Q. Tran, D. Jewell, H.M. Duong, A.M. Marconnet, Continuous Carbon Nanotube-Based Fibers and Films for Applications Requiring Enhanced Heat Dissipation, ACS Appl. Mater. Interfaces 8 (2016) 17461-17471.

[10] E. Huttunen, M.T. Nykänen, J. Alexandersen, Material extrusion additive manufacturing and experimental testing of topology-optimised passive heat sinks using a thermally-conductive plastic filament, Addit. Manuf. 59 (2022) 103123.

[11] M. Smith, S. Kim, A. Lambert, M. Walde, J. Lindahl, K. Mungale, T. Bougher, A.A. Hassen, V. Kunc, Maximizing the Performance of a 3D Printed Heat Sink by Accounting for Anisotropic Thermal Conductivity During Filament Deposition, 2019 18th IEEE Intersociety Conference on Thermal and Thermomechanical Phenomena in Electronic Systems (ITherm), 2019, pp. 626-632.

[12] H. Guo, H. Niu, H. Zhao, L. Kang, Y. Ren, R. Lv, L. Ren, M. Maqbool, A. Bashir, S. Bai, Highly Anisotropic Thermal Conductivity of Three-Dimensional Printed Boron Nitride-Filled Thermoplastic Polyurethane Composites: Effects of Size, Orientation, Viscosity, and Voids, ACS Appl. Mater. Interfaces 14 (2022) 14568-14578.

[13] A.G. Crowley, T.Q. Tran, M.J. Green, Using nanomaterials to enhance the additive manufacturing of polymeric resins, Nano Futures 6 (2022) 042502.

[14] A. Sarmah, S.K. Desai, A.G. Crowley, G.C. Zolton, G.B. Tezel, E.M. Harkin, T.Q. Tran, K. Arole, M.J. Green, Additive manufacturing of nanotube-loaded thermosets via direct ink writing and radio-frequency heating and curing, Carbon 200 (2022) 307-316.

[15] T.Q. Tran, X. Deng, C. Canturri, C.L. Tham, F.L. Ng, Highly-dense acrylonitrile butadiene styrene specimens fabricated by overheat material extrusion 3D printing, Rapid Prototyp. J. 29 (2023) 687-696.

[16] T.Q. Tran, F.L. Ng, J.T.Y. Kai, S. Feih, M.L.S. Nai, Tensile Strength Enhancement of Fused Filament Fabrication Printed Parts: A Review of Process Improvement Approaches and Respective Impact, Addit. Manuf. 54 (2022) 102724.

[17] F.L. Ng, T.Q. Tran, T. Liu, A methodology to develop part acceptance criteria model using non-destructive inspection technique for FDM printed part, Mater. Today: Proc. 70 (2022) 310-316.

[18] M.C. Vu, T.H. Jeong, J.B. Kim, W.K. Choi, D.H. Kim, S.R. Kim, 3D printing of copper particles and poly(methyl methacrylate) beads containing poly(lactic acid) composites for enhancing thermomechanical properties, J. Appl. Polym. Sci. 138 (2021) 49776.

[19] N. Nguyen, E. Melamed, J.G. Park, S. Zhang, A. Hao, R. Liang, Direct Printing of Thermal Management Device Using Low-Cost Composite Ink, Macromol. Mater. Eng. 302 (2017) 1700135.

[20] N. Nguyen, S. Zhang, A. Oluwalowo, J.G. Park, K. Yao, R. Liang, High-Performance and Lightweight Thermal Management Devices by 3D Printing and Assembly of Continuous Carbon Nanotube Sheets, ACS Appl. Mater. Interfaces 10 (2018) 27171-27177.

[21] R.D. Maalihan, Q. Chen, H. Tamura, J.R.H. Sta. Agueda, B.B. Pajarito, E.B. Caldona, R.C. Advincula, Mechanically and Thermally Enhanced 3D-Printed Photocurable Polymer Nanocomposites Containing Functionalized Chitin Nanowhiskers by Stereolithography, ACS Appl. Polym. Mater. 4 (2022) 2513-2526.

[22] C.P. Feng, K.Y. Sun, J.C. Ji, L. Hou, G.P. Cui, Z.G. Zhao, H.B. Lan, 3D Printable, form stable, flexible phase-change-based electronic packaging materials for thermal management, Addit. Manuf. 71 (2023) 103586.

[23] K. Timbs, M. Khatamifar, E. Antunes, W. Lin, Experimental study on the heat dissipation performance of straight and oblique fin heat sinks made of thermal conductive composite polymers, Therm. Sci. Eng. Prog. 22 (2021) 100848.

[24] H.Y. Zhao, M.Y. Yu, J. Liu, X. Li, P. Min, Z.Z. Yu, Efficient Preconstruction of Three-Dimensional Graphene Networks for Thermally Conductive Polymer Composites, Nano-Micro Lett. 14 (2022) 129.

[25] A. Sarmah, S.K. Desai, G.B. Tezel, A. Vashisth, M.M. Mustafa, K. Arole, A.G. Crowley, M.J. Green, Rapid Manufacturing via Selective Radio-Frequency Heating and Curing of Thermosetting Resins, Adv. Eng. Mater. 24 (2022) 2101351.

[26] N.S. Hmeidat, J.W. Kemp, B.G. Compton, High-strength epoxy nanocomposites for 3D printing, Compos. Sci. Technol. 160 (2018) 9-20.

[27] E.C. Murphy, J.H. Dumont, C.H. Park, G. Kestell, K.S. Lee, A. Labouriau, Tailoring properties and processing of Sylgard 184: Curing time, adhesion, and water affinity, J. Appl. Polym. Sci. 137 (2020) 48530.

[28] A. Vashisth, R.E. Healey, M.J. Pospisil, J.H. Oh, M.J. Green, Continuous processing of pre-pregs using radio frequency heating, Compos. Sci. Technol. 195 (2020) 108211.

[29] A. Sarmah, M.A. Morales, A. Srivastava, S. Upama, A. Nandi, T.C. Henry, M.J. Green, A. Vashisth, Interfacial carbon fiber–matrix interactions in thermosetting composites volumetrically cured by electromagnetic fields, Compos. Part A Appl. Sci. Manuf. 164 (2023) 107276.

[30] S.S. Dasari, A. Sarmah, R.D. Mee, A.N. Khalfaoui, M.J. Green, Joule Heating of Carbon Fibers and Their Composites in Radio-Frequency Fields, Adv. Eng. Mater. 25 (2023) 2201631.

[31] N. Patil, X. Zhao, N.K. Mishra, M.A. Saed, M. Radovic, M.J. Green, Rapid Heating of Silicon Carbide Fibers under Radio Frequency Fields and Application in Curing Preceramic Polymer Composites, ACS Appl. Mater. Interfaces 11 (2019) 46132-46139.

[32] C.B. Sweeney, B.A. Lackey, M.J. Pospisil, T.C. Achee, V.K. Hicks, A.G. Moran, B.R. Teipel, M.A. Saed, M.J. Green, Welding of 3D-printed carbon nanotube-polymer composites by locally induced microwave heating, Sci. Adv. 3 (2017) e1700262.

[33] C.B. Sweeney, A.G. Moran, J.T. Gruener, A.M. Strasser, M.J. Pospisil, M.A. Saed, M.J. Green, Radio Frequency Heating of Carbon Nanotube Composite Materials, ACS Appl. Mater. Interfaces 10 (2018) 27252-27259.

[34] I. Enriquez, C. Noronha, K. Teo, A. Sarmah, S. Gupta, A. Nandi, B. Fishbeck, M.J. Green, A. Vashisth, Closed-Loop Composite Welding and Bonding System Using Radio-Frequency Heating and Pressure, J. Compos. Sci., 2023.

[35] J.H. Oh, A.D. Martinez, H. Cao, G.W. George, J.S. Cobb, P. Sharma, L.A. Fassero, K. Arole, M.A. Carr, K.M. Lovell, J. Shukla, M.A. Saed, R. Tandon, M.E. Marquart, L.C. Moores, M.J. Green, Radio Frequency Heating of Washable Conductive Textiles for Bacteria and Virus Inactivation, ACS Appl. Mater. Interfaces 14 (2022) 43732-43740.

[36] D. Debnath, X. Zhao, M. Anas, D.L. Kulhanek, J.H. Oh, M.J. Green, Radio frequency heating and reduction of Graphene Oxide and Graphene Oxide - Polyvinyl Alcohol Composites, Carbon 169 (2020) 475-481.

[37] M. Conrad, A. Diatlov, R.W. DeDoncker, Implementation aspects of on-chip printed micro heat sinks for power semiconductors, 2015 IEEE Energy Conversion Congress and Exposition (ECCE), 2015, pp. 5716-5723.

[38] S. Derakhshanfar, R. Mbeleck, K. Xu, X. Zhang, W. Zhong, M. Xing, 3D bioprinting for biomedical devices and tissue engineering: A review of recent trends and advances, Bioact. Mater. 3 (2018) 144-156.

[39] A. Maqsood, M. Anis-ur-Rehman, Transient plane source (tps) sensors for simultaneous measurements of thermal conductivity and thermal diffusivity of insulators, fluids and conductors, IOP Conf. Ser.: Mater. Sci. Eng. 51 (2013) 012006.

[40] S. Diener, G. Franchin, N. Achilles, T. Kuhnt, F. Rösler, N. Katsikis, P. Colombo, X-ray microtomography investigations on the residual pore structure in silicon nitride bars manufactured by direct ink writing using different printing patterns, Open Ceram. 5 (2021) 100042.

[41] M.M. Abdelhamied, A.M. Abdelreheem, A. Atta, Influence of ion beam and silver nanoparticles on dielectric properties of flexible PVA/PANI polymer composite films, Plast. Rubber Compos. 51 (2022) 1-12.

[42] J.H. Oh, G.W. George, A.D. Martinez, L.C. Moores, M.J. Green, Radio frequency heating of PEDOT:PSS, Polymer 230 (2021) 124077.

[43] C.M. University, Hot electronics, 2021. https://www.ece.cmu.edu/news-and-events/story/2021/06/hot-electronics.html. (Accessed April 30 2023).

[44] T. Bardelli, C. Marano, F. Briatico Vangosa, Polydimethylsiloxane crosslinking kinetics: A systematic study on Sylgard184 comparing rheological and thermal approaches, J. Appl. Polym. Sci. 138 (2021) 51013.

[45] C. Techologies, The Operating Temperature For A Raspberry Pi, 2020. https://copperhilltech.com/content/The%20Operating%20Temperature%20For%20A%20Raspberry%20Pi%20%E2%80%93%20Technologist%20Tips.pdf. (Accessed April 30 2023).

[46] Y. Joo, S.J. Kim, Comparison of thermal performance between plate-fin and pin-fin heat sinks in natural convection, Int. J. Heat Mass Transf. 83 (2015) 345-356.

[47] E.C. Silva, Á.M. Sampaio, A.J. Pontes, Evaluation of Active Heat Sinks Design under Forced Convection—Effect of Geometric and Boundary Parameters, Materials 14 (2021) 2041.